

# RSC Advances



This is an *Accepted Manuscript*, which has been through the Royal Society of Chemistry peer review process and has been accepted for publication.

*Accepted Manuscripts* are published online shortly after acceptance, before technical editing, formatting and proof reading. Using this free service, authors can make their results available to the community, in citable form, before we publish the edited article. This *Accepted Manuscript* will be replaced by the edited, formatted and paginated article as soon as this is available.

You can find more information about *Accepted Manuscripts* in the [Information for Authors](#).

Please note that technical editing may introduce minor changes to the text and/or graphics, which may alter content. The journal's standard [Terms & Conditions](#) and the [Ethical guidelines](#) still apply. In no event shall the Royal Society of Chemistry be held responsible for any errors or omissions in this *Accepted Manuscript* or any consequences arising from the use of any information it contains.

**A facile one-pot dealloying strategy to synthesize monolithic  
asymmetry-patterned nanoporous copper ribbons with tunable  
microstructure and nanoporosity**

Wenbo Liu,<sup>1,a,b,\*</sup> Chenglai Xin,<sup>1,a</sup> Long Chen,<sup>a</sup> Jiazhen Yan,<sup>a</sup> Ning Li,<sup>a</sup> Sanqiang Shi,<sup>b</sup>

Shichao Zhang<sup>c</sup>

<sup>a</sup> School of Manufacturing Science and Engineering, Sichuan University, Chengdu  
610065, China

<sup>b</sup> Department of Mechanical Engineering, The Hong Kong Polytechnic University,  
Hung Hom, Kowloon, Hong Kong

<sup>c</sup> School of Materials Science and Engineering, Beihang University, Beijing  
100191, China

<sup>1</sup> These authors contributed equally.

Tel: +86-028-85405320; Fax: +86-028-85403408; E-mail: liuwenbo\_8338@163.com.

**Abstract**

In the present work, an effective and facile one-pot dealloying strategy has been developed to synthesize monolithic asymmetry-patterned nanoporous copper ribbons (AP-NPCRs) from melt-spun bi-phase Al 32 at.% Cu alloy with a trace  $\alpha$ -Al. The microstructure and nanoporosity of these AP-NPCRs were characterized using X-ray diffraction, scanning electron microscopy, energy dispersive X-ray analysis, transmission electron microscopy, high-resolution transmission electron microscopy, and Brunauer-Emmett-Teller. The results show that the cooling rate and dealloying solution have a significant influence on formation, microstructure and nanoporosity of AP-NPCRs. The quenching surface of porous products has regular bimodal channel size distributions regardless of corrosive solution species, while the free surface shows homogeneous porous network nanostructure in the acidic solution and anomalous bimodal nanoporous architecture in the alkaline medium. Additionally, microstructure (surface morphology, ligament/channel sizes and distribution) and nanoporosity of AP-NPCRs can be modulated effectively by simply changing dealloying solution.

**Keywords:** One-pot dealloying; Nanoporous copper; asymmetrical pattern; Microstructure; Nanoporosity

## 1. Introduction

Nanoporous metals (NPMs), as novel functional materials, have recently attracted great interest for their wide applications in catalysis, sensors, actuators, heat exchangers, supercapacitors, and so forth, owing to their unique physical, chemical, and mechanical properties associated with their high surface-to-volume ratio and low densities.<sup>1-8</sup> For a long time past, template methods are commonly used to fabricate these materials through the replication of porous alumina or liquid-crystal templates.<sup>9-11</sup> Since it has been found that chemical/electrochemical dealloying can be used to yield a broad range of porous metals, during the latest decades, a great deal of effort has been directed towards the investigation of NPMs prepared through dealloying.<sup>12-15</sup> Currently, one of the most important issues on research of NPMs is synthesis. Typically, normal dealloying methods to porous metals with controlled pore sizes result in formation of porous products with a narrow- or single-sized range, for instance, 200 nm for nanoporous copper (NPC),<sup>16</sup>  $225 \pm 53$  nm for nanoporous silver (NPS),<sup>17</sup> and 13 nm for nanoporous gold (NPG).<sup>18</sup> Obviously, a multimodal porous architecture can impart multi-functionalization and enhanced properties to porous materials. For instance, large-sized channels can favor increased mass transport while small-sized channels can improve activity due to their high specific surface area.

Ding et al.<sup>19</sup> reported on a two-step dealloying strategy to make free-standing noble metal membranes with a typical bimodal pore size distribution by performing a annealing-redealloying cycle on Ag-plated NPG. However, the cycle markedly prolongs the production time and increases the cost. Recently, our group developed an

effective one-pot route to fabricate the NPMs with hierarchical pore size distributions via modulating surface diffusivity of more noble elements along alloy/solution interfaces.<sup>20</sup> Compared to the previous two-step strategy, the one-pot route has evident advantages of simplicity and economy. Thus, avoiding cycling treatment and achieving facile synthesis of multimodal nanoporous architecture are crucial for its wider applications, which urgently need to be investigated.

It is well recognized that porosity evolution during dealloying involves etching of the base metal coupled with coarsening of the noble metal by surface diffusion.<sup>14,21</sup> Obviously, aside from the above-mentioned modulation of surface diffusivity, adjusting and controlling the etching-related process during dealloying also could be an alternative way to achieve the target. As is well-known, phase constituent and distribution in multi-phase alloys play a crucial role in the formation of NPMs and have a key influence on its microstructure and nanoporosity.<sup>22</sup> Inspired by it, a specific strategy towards the realization of goal could be proposed through designing the phase constituent and adjusting the phase distribution of initial alloys, as well as controlling the subsequent one-step dealloying behavior.

In this report, the well-designed bi-phase Al 32 at.% Cu alloy with a trace amount of  $\alpha$ -Al phase (typical composition of divorced eutectic structure; for comparison, up to 33 at.% Cu corresponding to just a single-phase Al<sub>2</sub>Cu alloy) was taken to synthesize the novel monolithic nanoporous copper with asymmetry-patterned porous microstructure through one-pot chemical dealloying. The experimental results show that the cooling rate and dealloying solution have a significant influence on the

formation, microstructure (surface morphology, ligament/channel sizes and distribution) and nanoporosity of the AP-NPCRs. The quenching surface of the NPCRs exhibits regular bimodal channel size distributions irrespective of dealloying solution species, while the free surface shows homogeneous porous network nanostructure in the acidic medium and anomalous bimodal nanoporous architecture in the alkaline corrosive circumstance. Just the great microstructure discrepancy between quenching and free surfaces of the resultant porous products constitutes the unique asymmetry-patterned characteristics. Additionally, microstructure and nanoporosity of the AP-NPCRs can be effectively tuned by simply changing dealloying solution. Based on our current understanding of underlying physical nature of dealloying of multi-phase alloys, the formation mechanism has been discussed in detail.

## 2. Experimental Section

Al-Cu alloy with nominal composition of 32 at.% Cu was prepared from pure Al (99.99 wt.%) and pure Cu (99.999 wt.%). Voltaic arc heating was employed to melt the charges in a copper crucible under an argon atmosphere, and then the melt was cooled down into ingots in situ. By use of a single roller melt spinning apparatus, the Al-Cu ingots were remelted in a quartz tube by high-frequency induction heating and then melt-spun onto a copper roller at a circumferential speed of ~3000 rpm in a controlled argon atmosphere. The alloy ribbons obtained were typically 10-20  $\mu\text{m}$  in thickness, 4-6 mm in width, and several centimeters in length. It should be pointed out that, during solidification, two surfaces of the alloy ribbons actually subjected to remarkably different cooling rates: the rate of surface directly contacting with copper

roller is much higher due to the intrinsic heat transfer property of copper relative to the other contacting with Ar, which thereby was distinguished as the quenching surface and free surface, respectively. Energy dispersive X-ray (EDX) analysis showed the atomic percentage of Cu and Al in the initial Al-Cu alloy was quite closely to the designed chemical composition, indicating the alloy ribbons can be further used in the following experiment. Subsequently, the melt-spun Al-Cu alloy ribbons were dealloyed in a 5 wt.% HCl aqueous solution at 75°C or 10 wt.% NaOH aqueous solution at 15°C until no obvious bubbles emerged, respectively. After dealloying, the samples were rinsed with distilled water and dehydrated alcohol several times, and then kept in a vacuum chamber to avoid oxidation.

Microstructural characterization and analysis of the melt-spun Al-Cu alloy ribbons and as-dealloyed samples were made using X-ray diffraction (XRD, Rigaku D/Max-2400) with Cu K $\alpha$  radiation, scanning electron microscopy (FESEM, Hitachi S-4800) with an EDX analyzer, transmission electron microscopy (TEM, JEOL JEM 2100F) with selected-area electron diffraction (SAED). To test the electrochemical activities of  $\alpha$ -Al and Al<sub>2</sub>Cu phases in the Al 32 at.% Cu alloy, potentiodynamic polarization studies were conducted on single-phase  $\alpha$ -Al solid solution and Al<sub>2</sub>Cu intermetallics (corresponding to Al-Cu alloy with a trace amount of Cu and Al 33 at.% Cu alloy by the same preparation procedure mentioned above) in the different corrosive environments by using an electrochemical measurement unit (PARSTAT 2273). The experiments were carried out in a standard three-electrode electrochemical cell (200 mL) with a Pt plate electrode as a counter electrode, a saturated calomel

electrode (SCE) as a reference electrode, and the alloy ribbon as the working electrode. Polarization scan was performed towards positive values at a scan rate of  $1.0 \text{ mV s}^{-1}$ , after allowing a steady state potential to develop. In order to evaluate specific surface areas of these NPCRs prepared under different dealloying conditions, the  $\text{N}_2$  adsorption/desorption experiments were carried out at 77 K on a Nova Station A automatic surface area and pore radius distribution apparatus.

### 3. Results

Figure 1 shows the XRD patterns of the initial melt-spun Al 32 at.% Cu alloy ribbons and their as-dealloyed samples upon the dealloying in the HCl/NaOH solution. The filled circles, squares and triangles stand for  $\alpha$ -Al,  $\text{Al}_2\text{Cu}$  and Cu, respectively. As can be seen from Figure 1a, the Al 32 at.% Cu alloy is composed of  $\alpha$ -Al and  $\text{Al}_2\text{Cu}$  phases, and the amount of  $\text{Al}_2\text{Cu}$  is overwhelmingly dominant in contrast to just a trace amount of  $\alpha$ -Al in the initial alloy. Upon the dealloying in the 5 wt.% HCl at  $75^\circ\text{C}$ /10 wt.% NaOH solution at  $15^\circ\text{C}$  (bubbling ceased), only a face-centered cubic (f.c.c.) Cu phase can be identified in the as-dealloyed samples, as presented in Figure 1b-c. It should be noted that, however, the peak width of  $(111)_{\text{Cu}}$ ,  $(200)_{\text{Cu}}$ ,  $(220)_{\text{Cu}}$  reflections of the resultant porous products by dealloying in the alkaline solution is significantly broad in comparison with that in the acidic medium, suggesting that the length scales of porous structures in the NPCRs by dealloying in the NaOH solution are much smaller.<sup>23</sup>

The quenching surface of the NPCRs from Al 32 at.% Cu alloy shows that a porous structure with regular bimodal channel size distributions can be obtained upon the

dealloying in the HCl solution and typical SEM images are shown in Figure 2a-b. Clearly, the quenching surface exhibits a regular bimodal ligament-channel network structure composed of interconnected large-sized annular channels ( $150 \pm 50$  nm) encircling with island-shaped porous channel walls. The SEM image at a higher magnification displays the island-shaped channel walls show an open, bicontinuous interpenetrating porous network with ligament sizes of  $50 \pm 10$  nm (Figure 2b). Astonishingly, the free surface of the NPCRs shows homogeneous porous nanostructure can be obtained under the same dealloying conditions and a typical SEM image is presented in Figure 2c. The high-magnification SEM image clearly exhibits a uniformly bicontinuous porous network with ligament/channel sizes of  $50 \pm 10$  nm (Figure 2d). Thus, the as-made monolithic NPCRs have asymmetrically patterned porous structure features composed of regular bimodal channel size distributions on the quenching surface coupled with a homogeneous porous network nanostructure on the free surface upon the dealloying in the acidic solution. Herein, we define the unique NPCRs with asymmetry-patterned porous structures on the free and quenching surfaces as AP-NPCRs. This unique kind of porous structure is considered to be considerably significant for the wide application of electrochemical biosensors and actuators due to the special distribution model of channels on the surfaces, in which the bimodal porous network is beneficial for the fast penetration of electrolyte throughout whole samples, while the homogeneous one is desirable in increasing device sensitivity. EDX analysis has been performed on the NPCRs and one typical spectrum is shown in Figure 3e. Obviously, nearly all of Al was removed

from the Al-Cu alloy upon dealloying in the HCl solution. In contrast, NPG (by dealloying of Ag-Au alloys in a HNO<sub>3</sub> solution) normally contains some residual at.% Ag, which is expected to be trapped inside the Au ligaments based upon the dealloying mechanism and cannot be removed but asymptotically reaches a limit at exhaustively long etching times (up to 100 h).<sup>24,25</sup>

TEM observation further verifies the porous structure of the NPCRs by dealloying in the HCl solution and one typical TEM bright-field image is shown in Figure 3a. Clearly, the high-magnification TEM image shows the small-sized ligament edges are coarse and accumulated by nanoparticles with a size of several to tens of nm, as shown in Figure 3b. A SAED pattern consists of polycrystalline rings, corresponding to f.c.c. (111)<sub>Cu</sub>, (200)<sub>Cu</sub>, (220)<sub>Cu</sub>, and (311)<sub>Cu</sub> reflections, respectively (inset of Figure 3a). Moreover, the crossed lattice fringes on the outmost surface of ligament from the HRTEM image in Figure 3c further demonstrate that the ligaments in the NPCRs comprise Cu polycrystals rather than the monocrystals typically observed in the ligaments of NPG through dealloying of the prototypical Ag-Au system,<sup>26</sup> which is probably related to the secondary nucleation caused by greater mobility of Cu atoms (than that of Au atoms).<sup>27-31</sup>

In this work, it also has been found that the microstructure and porosity of AP-NPCRs can be adjusted effectively by changing the dealloying solution. Figure 4 shows the microstructures on the quenching and free surfaces of the AP-NPCRs upon dealloying of the melt-spun Al 32 at.% Cu alloy in the 10 wt.% NaOH solution at 15°C. As can be seen from Figure 4a, the quenching surface exhibits a quite similar

microstructure feature to that obtained in the HCl solution with the exception of the slightly larger sizes of annular channels, that is a regular bimodal porous nanostructure composed of interconnected large-sized annular channels ( $200\pm 50$  nm) encircling with island-shaped channel walls. The SEM image at a higher magnification shows the channel walls exhibit a uniform, bicontinuous interpenetrating porous network with ligament sizes of  $20\pm 5$  nm (Figure 4b). In contrast, anomalous bimodal nanoporous architectures can be achieved on the free surface of the NPCRs, which consists of interconnected large-sized river-shape channels with uniformly porous channel walls. The large-sized river-shape channels with length scales of  $800\pm 200$  nm can be clearly seen on the free surface of the NPCRs, as shown in Figure 4c. The high-magnification SEM image displays the river-shape channel walls also comprise a uniform, bicontinuous interpenetrating ligament-channel network with length scales of  $20\pm 5$  nm, as good as that observed on the quenching surface (Figure 4d). As a consequence, the as-prepared NPCRs have asymmetrically patterned porous structure features composed of regular bimodal channel size distributions on the quenching surface and anomalous bimodal porous nanonetworks on the free surface upon dealloying in the alkaline medium, which also possesses potential dual-functionalization in the biosensing and actuating applications. It is worth noting that the length scales of ligaments/channels in the uniformly porous channel walls of the NPCRs, whether on the quenching or free surfaces, by dealloying in the alkaline solution are much smaller than those in the acidic medium, which also has been found by the remarkable increase of peak width of reflections in the XRD

results due to its more sensitive to the change in structure size of Cu phase. Additionally, EDX analysis shows only Cu can be identified and nearly all of Al was etched away during dealloying in the NaOH solution (Figure 4e).

Figure 5a shows the typical TEM image of porous structure of the NPCRs by dealloying in the NaOH solution. The length scales of ligaments/channels are in good agreement with the SEM observations. Obviously, the smooth ligament edges can be observed clearly in the high-magnification TEM image (Figure 5b) in comparison with the coarse one obtained in the acidic solution, indicating that dealloying solution has a significant effect on the surface morphology of NPCRs. The SAED pattern corresponding to one ligament is from the f.c.c. Cu [110] zone axis, indicating a single crystalline characteristic of the selected area (inset of Figure 5a). Moreover, lattice fringes extending throughout the whole ligament from the HRTEM image in Figure 5c further verify the single crystal nature of the small-sized ligament in the channel walls of NPCRs. It should be noted that, however, the present results are essentially different from the established notion that the crystal lattice orientation is retained during dealloying of Ag-Au solid solutions with the conservation of the grain size of the initial alloys.<sup>26,32-34</sup> For the lattice structure of the resultant NPCRs is considerably different from that of Al<sub>2</sub>Cu intermetallics in the initial Al-Cu alloy (Al<sub>2</sub>Cu: body centered tetragonal; Cu: f.c.c.).

Figure 6 shows Tafel polarization curves of single-phase  $\alpha$ -Al solid solution and Al<sub>2</sub>Cu intermetallics in the HCl and NaOH solutions, respectively. It can be found that in the alkaline solution, the difference between corrosion potentials of single-phase

$\alpha$ -Al solid solution and Al<sub>2</sub>Cu intermetallics is ~299 mV(SCE), much greater than that in the acidic solution (~9.91 mV(SCE)). The present results clearly indicate that  $\alpha$ -Al and Al<sub>2</sub>Cu have the close electrochemical activities in the acidic solution, while a relatively high electrochemical activity can be obtained for  $\alpha$ -Al in the alkaline solution compared to Al<sub>2</sub>Cu.

The specific surface areas of these NPCRs have been evaluated based upon N<sub>2</sub> adsorption/desorption experiments. Figure 7 shows the N<sub>2</sub> adsorption/desorption isotherms for the NPCRs by dealloying of the bi-phase Al 32 at.% Cu alloy in the 5 wt.% HCl/10 wt.% NaOH solution. The Brunauer-Emmett-Teller surface areas of the resultant porous products by dealloying in the acidic/alkaline solution are quite high and have been determined to be  $17.2 \pm 0.1$  and  $30.6 \pm 0.1$  m<sup>2</sup> g<sup>-1</sup>, which would be especially beneficial for biosensing and actuating applications.

#### 4. Discussion

It is generally recognized that ideal bicontinuous nanoporous structures are obtained from binary alloy families with a single-phase solid solubility across all compositions by chemical/electrochemical dealloying. The formation mechanism of nanoporous structures during dealloying has been described in the literature.<sup>12</sup> It has been shown that ligaments form as a result of an intrinsic pattern formation during which aggregation of chemically driven noble metal atoms occurs. The process started with selective dissolution of base metal atoms from the outermost alloy surface, leaving behind noble metal atoms that diffused along alloy/solution interfaces and agglomerated into the ligaments. Thus, porosity evolution forms dynamically during

dissolution and is not due to one active component simply being excavated out of a binary solid solution alloy.<sup>35</sup>

However, if multiple phases exist in an alloy, a more complicated process will occur during dealloying. Typically, in a bi-phase alloy, if one phase can be entirely dissolved and another is just partly corroded, the dealloying of the alloy can lead to NPMs with bimodal channel size distributions, like the case for bimodal NPG.<sup>36,37</sup> The present Al-Cu alloy ribbons are composed of a combination of  $\alpha$ -Al and  $\text{Al}_2\text{Cu}$  phases, in which  $\alpha$ -Al phase can be entirely dissolved while  $\text{Al}_2\text{Cu}$  phase just may be selectively corroded, resulting theoretically into the formation of NPCRs with bimodal channel size distributions. On the other hand, as mentioned above, phase distribution in the initial alloy with multiple phases has a key influence on the microstructure of as-dealloyed products, which to a large extent depends on the solidification process of multi-phase alloy. In this case, the quenching surface of the melt-spun Al 32 at.% Cu alloy ribbons virtually experiences an essentially different solidification process relative to the free one because of its faster cooling rate, resulting in the occurrence of special solidification behavior and phase distribution state distinctive from that of free surface. As a result, the unique asymmetry-patterned porous architecture can be obtained upon the dealloying, indicating that cooling rate during the solidification of multi-phase alloy has a key role on the microstructure of NPCRs. The detailed formation mechanism is discussed as follows.

According to the non-equilibrium solidification theory, during the solidification of quenching surface of the Al 32 at.% Cu alloy, primary  $\text{Al}_2\text{Cu}$  phases can precipitate

firstly and the  $\alpha$ -Al solid solution subsequently forms from the remaining liquid, suppressing the occurrence of eutectic reaction due to the fast cooling rate. The microstructure on the quenching surface can be described as the annular  $\alpha$ -Al in the region of grain boundary (GB) surrounding the island-shaped primary  $\text{Al}_2\text{Cu}$  grains, namely divorced eutectic structure. Contrarily, during the solidification of free surface contacting with Ar, eutectics of  $\alpha$ -Al and  $\text{Al}_2\text{Cu}$  phases, typically for an alternating laminated structure with high free energy and low structure stability, can directly nucleate and continually grow from the initial liquid after the precipitation of primary  $\text{Al}_2\text{Cu}$  phase due to the relatively slow cooling rate, characteristic of hypereutectic structure. As a result of a combination of the above-mentioned two aspects, the Al 32 at.% Cu alloy ribbons have uniquely asymmetrical microstructure features composed of divorced eutectic structure on the quenching surface and hypereutectic structure on the free surface.

During the etching of quenching surface,  $\alpha$ -Al and  $\text{Al}_2\text{Cu}$  phases in divorced eutectic structure are prone to be separately dealloyed due to the relatively stable phase distribution state,<sup>38</sup> in which the excavation of the  $\alpha$ -Al in the region of GB contributes to the formation of large-sized annular channels, while the dealloying of the island-shaped  $\text{Al}_2\text{Cu}$  intermetallics results in the nanoporous structure of the large-sized channel walls, thereby forming the regular bimodal porous nanonetworks composed of interconnected large-sized annular channels with island-shaped porous channel walls. Obviously, this is in good agreement with the SEM observations on the quenching surface. Additionally, it can be reasonable to speculate that the morphology,

size, and distribution of these large-sized annular channels and island-shaped porous structures inherit from those counterparts of  $\alpha$ -Al and  $\text{Al}_2\text{Cu}$  on the quenching surface of the initial alloy, and hence we also can further know the information of  $\alpha$ -Al and  $\text{Al}_2\text{Cu}$  phases on the quenching surface of the initial alloy from the SEM images upon the dealloying.

On the free surface, dealloying behavior of hypereutectic structure would be more complex, because dealloying process of laminated  $\alpha$ -Al and  $\text{Al}_2\text{Cu}$  phases in eutectics strongly depends on their electrochemical activities. As indicated in Figure 6, the disparity between electrochemical activities of  $\alpha$ -Al and  $\text{Al}_2\text{Cu}$  phases is very small in the HCl solution, indicating  $\alpha$ -Al and  $\text{Al}_2\text{Cu}$  in eutectics can be almost simultaneously dissolved. As a result of the synergetic dealloying of  $\alpha$ -Al and  $\text{Al}_2\text{Cu}$  phases and the fast surface diffusion of Cu atoms along the alloy/solution interfaces, a homogenous ligament-channel structure can be fabricated on the free surface upon the dealloying in the HCl solution, like the case for a uniform porous structure from Al-Ag alloy with analogous two phases:  $\alpha$ -Al and  $\text{Al}_2\text{Ag}$ .<sup>39</sup>

Contrarily, in the alkaline environment, the electrochemical activity of  $\alpha$ -Al phase is much higher than  $\text{Al}_2\text{Cu}$ .  $\alpha$ -Al and  $\text{Al}_2\text{Cu}$  phases existing in eutectics can form corrosion couple cells due to the large difference between electrochemical activities of two distinct phases, with the  $\alpha$ -Al phase (more active) acting as an anode and preferentially dissolving compared with the  $\text{Al}_2\text{Cu}$ . The preferential dissolution of  $\alpha$ -Al phase forms interconnected large-sized river-shape channels beneficial for the further penetration of corrosive solution throughout the whole structure and the

dealloying of  $\alpha$ -Al facilitates that of  $\text{Al}_2\text{Cu}$ . Subsequently, Al can be further etched in the  $\text{Al}_2\text{Cu}$ , resulting in the formation of a homogenous nanoporous network in the large-sized channel walls by right of fast surface diffusion and rearrangement of Cu atoms along alloy/solution interfaces. This is why an anomalous bimodal nanoporous architecture composed of interconnected large-sized river-shape channels with uniformly porous channel walls can be obtained on the free surface of NPCRs upon dealloying in the NaOH solution. Obviously, this is in good agreement with the SEM observations, indicating that dealloying solution has a critical influence on the microstructure of NPCRs.

It is well-known that surface diffusion of more noble (MN) element along alloy/solution interfaces plays a key role in the formation of NPMs and has a significant influence on the length scales of ligaments/channels.<sup>12,35</sup> It has been found that the adsorption of chloride ion ( $\text{Cl}^-$ ) in acidic solution can greatly enhance the surface diffusion of MN atoms along alloy/solution interfaces during dealloying due to the modification of adsorbed bonds between neighboring sites via electron transfer reactions.<sup>21,33,40-41</sup> On the other hand, during the dealloying of Al-based alloys in alkali solution, surface diffusivity of MN atoms is much slower than that in acid media due to the formation of MN-hydroxy species, the interaction of MN atoms and  $\text{OH}^-$ , and the low solubility of  $\text{AlO}_2^-$ .<sup>42-44</sup> So in this case, it can be easier to understand that much higher surface diffusivity can be achieved in the HCl solution. This also will be further discussed based on the calculation on the surface diffusivity in the following section.

It has been reported that a maximally unstable spatial period relationship has been predicted for the characteristic length scale ( $d$ ) of nanoporous metals and surface diffusivity ( $D_s$ ):  $d \propto (D_s / V_0)^\mu$ , where  $V_0$  is the velocity of a flat alloy surface with no MN atoms accumulated upon it and  $\mu$  is a constant, suggested to be 1/6 or 1/4.<sup>12,45</sup> Based on the surface diffusion controlled coarsening mechanism, the  $D_s$  values of Cu atoms along alloy/solution interfaces can be estimated by the equation:<sup>45-46</sup>

$$D_s = \frac{[d(t)]^4 kT}{32\gamma t \alpha^4} \quad (1)$$

where  $k$  is the Boltzmann constant,  $\gamma$  is the surface energy ( $1.79 \text{ J m}^{-2}$ ),<sup>47</sup>  $d(t)$  is the ligament size at the dealloying time  $t$ ,  $\alpha$  is the lattice parameter of Cu ( $3.6153 \times 10^{-10} \text{ m}$ ), and  $T$  is the dealloying temperature. According to the ligament sizes in the channel walls of NPCRs, the  $D_s$  of Cu atoms along alloy/solution interfaces was calculated for dealloying of Al 32 at.% Cu alloy in the HCl/NaOH solution, as listed in Table 1. It is astonishing that the  $D_s$  of Cu atoms in the HCl solution,  $1.02 \times 10^{-16} \text{ m}^2 \text{ s}^{-1}$ , is three orders of magnitude greater than that in the NaOH solution although its dealloying duration is just 300 s, 1/72 of that in the alkaline medium, indicating the occurrence of substantial structure coarsening with greater surface diffusivity in the HCl solution. This is the reason that evidently small ligament-channel structure and quite large specific surface area can be achieved upon the dealloying in the alkaline solution. Note that in the former literature,<sup>35</sup> Erlebacher has theoretically estimated the  $D_s$  value of Cu atoms to be  $1.2 \times 10^{-14} \text{ m}^2 \text{ s}^{-1}$  in vacuum and inferred to be of order  $10^{-10} \text{ m}^2 \text{ s}^{-1}$  or faster in electrolyte. However, in

comparison with our experiment-based calculation results, it is an evidently overestimation, especially for the dealloying in the alkaline media.

Compared to most of NPMs with multimodal pore size distributions in the literature,<sup>19,20,37,38,48-52</sup> it is the first to report that the unique NPCRs with asymmetry-patterned porous microstructures can be obtained by the facile one-pot dealloying approach presented in this work. The microstructure and nanoporosity of products can be tuned effectively by simply changing the dealloying solution. Based on the present work, it can be proposed that this effective one-pot strategy can be extended to synthesize other monolithic asymmetry-patterned NPMs from designed bi-phase alloy systems. It will have important implications for fabricating excellent multi-functionalization electrode materials towards applications of electrochemical biosensors and actuators.

## 5. Conclusions

In summary, we present a simple and effective one-pot strategy to synthesize the monolithic asymmetry-patterned nanoporous copper ribbons by chemical dealloying of melt-spun bi-phase Al 32 at.% Cu alloy with a trace amount of  $\alpha$ -Al phase in the HCl/NaOH solution. The cooling rate and dealloying solution have a crucial influence on the formation, microstructure and nanoporosity of AP-NPCRs. The quenching surface of NPCRs has regular bimodal channel size distributions irrespective of dealloying solution species, while the free surface shows that homogeneous porous network nanostructure can be synthesized by dealloying in the acidic solution and anomalous bimodal nanoporous architecture can be achieved upon dealloying in the

alkaline medium. The formation of the unique DP-NPCRs originates from the great difference in distribution state of a trace  $\alpha$ -Al on the free and quenching surfaces induced by different cooling rates during the solidification of initial alloy, while the distinctive microstructures obtained in the acidic/alkaline solution are closely related to the large disparity between electrochemical activities of  $\alpha$ -Al and  $\text{Al}_2\text{Cu}$  phases in eutactics. Additionally, microstructure (surface morphology, ligament/channel sizes and distribution) and nanoporosity of the AP-NPCRs can be modulated effectively by changing the dealloying solution, which results from the different mobility of Cu atoms along the alloy/solution interfaces.

### Acknowledgements

We give thanks to financial support by the State Key Basic Research Program of PRC (2013CB934001), the National Natural Science Foundation of China (51274017, 51074011), the “HongKong Scholars Programme” Funded Project (XJ2014045, G-YZ67), the China Postdoctoral Science Foundation Funded Project (2015M570784), the Talent Introduction Fund Project of Sichuan University (YJ201410), and the Shanghai Aerospace Science & Technology Innovation Fund Project (SAST201269).

### References

- 1 V. Zielasek, B. Jurgens, C. Schulz, J. Biener, M. M. Biener, A. V. Hamza and M. Baumer, *Angew. Chem., Int. Ed.*, 2006, **45**, 8241.
- 2 C. F. Yu, F. L. Jia, Z. H. Ai and L. Z. Zhang, *Chem. Mater.*, 2007, **19**, 6065.
- 3 H. M. Yin, C. Q. Zhou, C. X. Xu, P. P. Liu, X. H. Xu and Y. Ding, *J. Phys. Chem.*

- C, 2008, **112**, 9673.
- 4 K. C. Hu, D. X. Lan, X. M. Li and S. S. Zhang, *Anal. Chem.*, 2008, **80**, 9124.
- 5 A. Mortari, A. Maarroof, D. Martin and M. B. Cortie, *Sens. Actuators. B*, 2007, **123**, 262.
- 6 F. Yu, S. Ahl, A. M. Caminade, J. P. Majoral, W. Knoll and J. Erlebacher, *Anal. Chem.*, 2006, **78**, 7346.
- 7 R. W. Ertenberg, B. Andraka and Y. Takano, *Physica B*, 2000, **2022**, 284.
- 8 M. B. Cortie, A. I. Maarroof and G. B. Smith, *Gold Bull.*, 2005, **38**, 14.
- 9 H. Masuda and K. Fukuda, *Science*, 1995, **268**, 1466.
- 10 G. S. Attard, P. N. Bartlett, N. R. B. Coleman, J. M. Elliott, J. R. Owen and J. H. Wang, *Science*, 1997, **278**, 838.
- 11 T. Kijima, T. Yoshimura, M. Uota, T. Ikeda, D. Fujikawa, S. Mouri and S. Uoyama, *Angew. Chem., Int. Ed.*, 2004, **43**, 228.
- 12 J. Erlebacher, M. J. Aziz, A. Karma, N. Dimitrov and K. Sieradzki, *Nature*, 2001, **410**, 450.
- 13 K. Sieradzki, N. Dimitrov, D. Movrin, C. McCall, N. Vasiljevic and J. Erlebacher, *J. Electrochem. Soc.*, 2002, **149**, B370.
- 14 C. X. Ji and P. C. Searson, *J. Phys. Chem. B*, 2003, **107**, 4494.
- 15 M. Stratmann and M. Rohwerder, *Nature*, 2001, **410**, 420.
- 16 X. Luo, R. Li, L. Huang and T. Zhang, *Corros. Sci.*, 2013, **67**, 100.
- 17 C. Zhang, J. Sun, J. Xu, X. Wang, H. Ji, C. Zhao and Z. Zhang, *Electrochim. Acta*, 2012, **63**, 302.

- 18 J. Zeng, F. Zhao, M. Li, C. Li, T. Lee and W. Shih, *J. Mater. Chem. C*, 2015, **3**, 247.
- 19 Y. Ding and J. Erlebacher, *J. Am. Chem. Soc.*, 2003, **125**, 7772.
- 20 W. B. Liu, S. C. Zhang, N. Li, J. W. Zheng and Y. L. Xing, *Micropor. Mesopor. Mater.*, 2011, **138**, 1.
- 21 Z. Qi, C. C. Zhao, X. G. Wang, J. K. Lin, W. Shao, Z. H. Zhang and X. F. Bian, *J. Phys. Chem. C*, 2009, **113**, 6694.
- 22 W. B. Liu, S. C. Zhang, N. Li, J. W. Zheng and Y. L. Xing, *Corros. Sci.*, 2011, **53**, 809.
- 23 W. B. Liu, S. C. Zhang, N. Li, J. W. Zheng and Y. L. Xing, *J. Electrochem. Soc.*, 2010, **157**, D666.
- 24 M. C. Dixon, T. A. Daniel, M. Hieda, D. M. Smilgies, M. H. W. Chan and D. L. Allara, *Langmuir*, 2007, **23**, 2414.
- 25 K. Sieradzki, R. R. Corderman and K. Shukla, *Phil. Mag. A*, 1989, **59**, 713.
- 26 Y. Ding, Y. J. Kim and J. Erlebacher, *Adv. Mater.*, 2004, **16**, 1897.
- 27 G. Madras and B. J. McCoy, *Chem. Eng. Sci.*, 2004, **59**, 2753.
- 28 C. Y. Tai, J. F. Wu and R. W. Rousseau, *J. Cryst. Growth*, 1992, **116**, 294.
- 29 M. S. Viola and G. D. Botsaris, *Chem. Eng. Sci.*, 1979, **34**, 993.
- 30 V. Repain, G. Baudot, H. Ellmer and S. Rousset, *Mater. Sci. Eng. B*, 2002, **96**, 178.
- 31 A. A. Schmidt, H. Eggers, K. Herwig and R. Anton, *Surf. Sci.*, 1996, **349**, 301.
- 32 Y. Ding, A. Mathur, M. W. Chen and J. Erlebacher, *Angew. Chem., Int. Ed.*, 2005, **44**, 4002.

- 33 S. Parida, D. Kramer, C. A. Volkert, H. Rö sner, J. Erlebacher and J. Weissm ü ller, *Phys. Rev. Lett.*, 2006, **97**, 035504.
- 34 A. J. Forty and P. Durkin, *Philos. Mag. A*, 1980, **42**, 295.
- 35 J. Erlebacher, *J. Electrochem. Soc.*, 2004, **151**, C614.
- 36 Z. H. Zhang, Y. Wang, Z. Qi, J. K. Lin and X. F. Bian, *J. Phys. Chem. C*, 2009, **113**, 1308.
- 37 Z. H. Zhang, Y. Wang, Z. Qi, W. H. Zhang, J. Y. Qin and J. Frenzel, *J. Phys. Chem. C*, 2009, **113**, 12629.
- 38 W. B. Liu, S. C. Zhang, N. Li, J. W. Zheng, S. S. An and Y. L. Xing, *Int. J. Electrochem. Sci.*, 2011, **6**, 5445.
- 39 X. G. Wang, Z. Qi, C. C. Zhao, W. M. Wang and Z. H. Zhang, *J. Phys. Chem. C*, 2009, **113**, 13139.
- 40 J. M. Dona and J. Gonzalez-Velasco, *Surf. Sci.*, 1992, **274**, 205.
- 41 J. M. Dona and J. Gonzalez-Velasco, *J. Phys. Chem.*, 1993, **97**, 4714.
- 42 W. B. Liu, L. Chen, J. Z. Yan, N. Li, S. Q. Shi and S. C. Zhang, *Corros. Sci.*, 2015, **94**, 114.
- 43 Z. H. Zhang, Y. Wang, Y. Z. Wang, X. G. Wang, Z. Qi, H. Ji and C. C. Zhao, *Scripta Mater.*, 2010, **62**, 137.
- 44 W. B. Liu, S. C. Zhang, N. Li, J. W. Zheng and Y. L. Xing, *J. Electrochem. Soc.*, 2011, **158**, D611.
- 45 L. H. Qian and M. W. Chen, *Appl. Phys. Lett.*, 2007, **91**, 083105.
- 46 G. Andreasen, M. Nazzarro, J. Ramirez, R. C. Salvarezza and A. J. Arvia, *J.*

- Electrochem. Soc.*, 1996, **143**, 466.
- 47 W. R. Tyson and W. A. Miller, *Surf. Sci.*, 1977, **62**, 267.
- 48 S. S. An, S. C. Zhang, W. B. Liu, H. Fang, M. L. Zhang and Y. Yu, *Corros. Sci.*, 2013, **75**, 256.
- 49 W. B. Liu, S. C. Zhang, N. Li, J. W. Zheng and Y. L. Xing, *Corros. Sci.*, 2012, **58**, 133-138.
- 50 Z. H. Zhang, C. Zhang, Y. L. Gao, J. Frenzel, J. Z. Sun and G. Eggeler, *CrystEngComm*, 2012, **14**, 8292.
- 51 W. B. Liu, S. C. Zhang, N. Li, J. W. Zheng, S. S. An and Y. L. Xing, *Int. J. Electrochem. Sci.*, 2012, **7**, 6365.
- 52 N. T. Tuan, J. Park, J. Lee, J. Gwak and D. Lee, *Corros. Sci.*, 2014, **80**, 7.

**Table 1.** The ligament sizes in the channel walls of NPCRs by dealloying of Al 32 at.% Cu alloy in the HCl/NaOH solution, the corresponding surface diffusivities estimated by Eq. (1).<sup>45-46</sup>

Dealloying solution	HCl	NaOH
Dealloying temperature (T, K)	348	288
Dealloying time (t, s)	300	21600
Ligament size in porous pore walls (d(t), nm)	50±5	20±5
Surface diffusivity ( $D_s$ , $m^2 s^{-1}$ )	$1.02 \times 10^{-16}$	$3.01 \times 10^{-20}$

### Figure Captions

Figure 1. XRD patterns of melt-spun Al 32 at.% Cu alloy ribbons (a) before and (b-c) upon dealloying in the 5 wt.% HCl at 75°C and 10 wt.% NaOH solution at 15°C, respectively.

Figure 2. SEM images showing the microstructure of (a, b) quenching surface, and (c, d) free surface of NPCRs by dealloying of the Al 32 at.% Cu alloy in the 5 wt.% HCl solution at 75°C. Insets in parts b and d are their high-magnification images. (e) A typical EDX spectrum shows the composition of the resultant NPCRs.

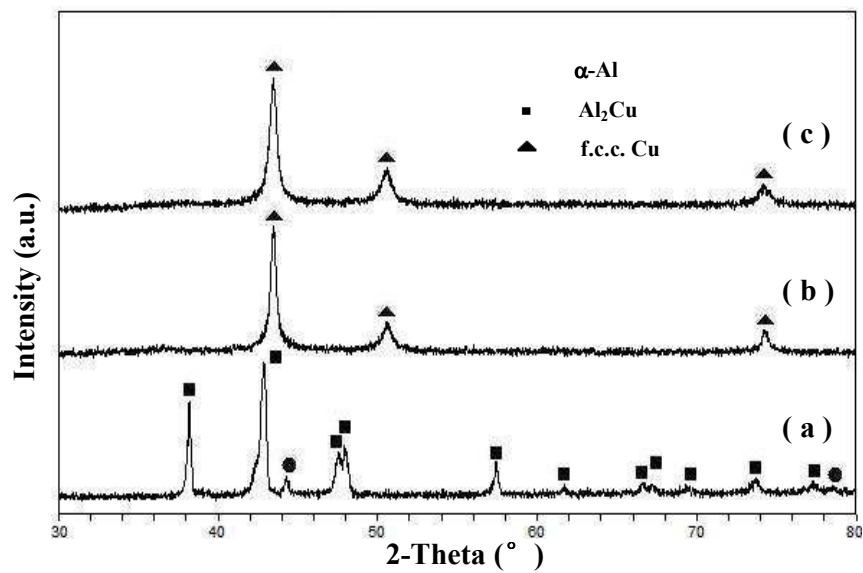
Figure 3. (a,b) TEM images show the porous structure in the channel walls of NPCRs by dealloying of melt-spun Al 32 at.% Cu alloy in the 5 wt.% HCl solution at 75°C; (inset) SAED pattern corresponding to a ligament in part a; part b shows the coarse ligament surface morphology at a higher magnification. (c) HRTEM image shows the crossed lattice fringes in the ligament.

Figure 4. SEM images showing the microstructure of (a, b) quenching surface, and (c, d) free surface of NPCRs by dealloying of the Al 32 at.% Cu alloy in the 10 wt.% NaOH solution at 15°C. Insets in parts b and d are their high-magnification images. (e) A typical EDX spectrum shows the composition of the resultant NPCRs.

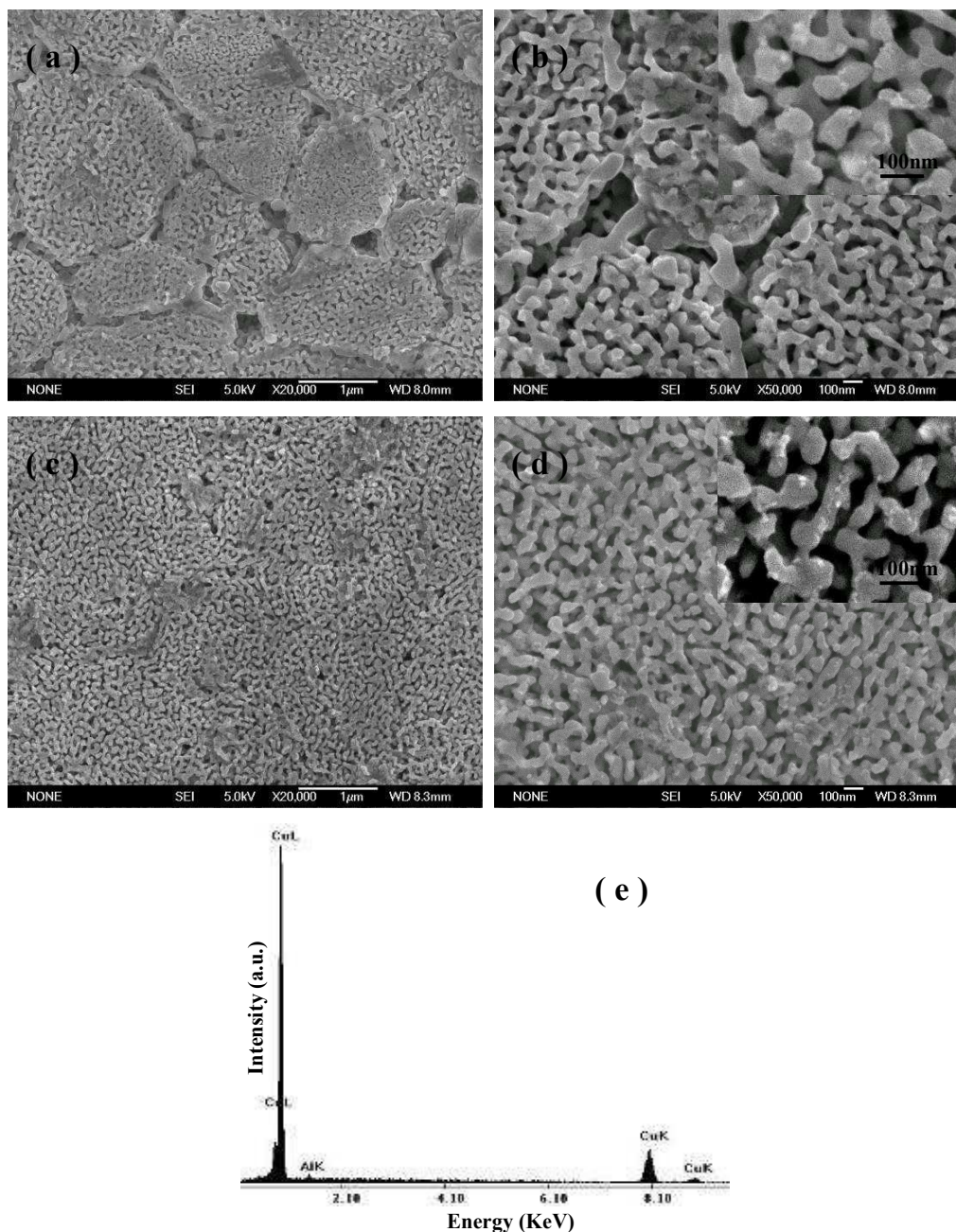
Figure 5. (a,b) TEM images show the porous structure in the channel walls of NPCRs by dealloying of melt-spun Al 32 at.% Cu alloy in the 10 wt.% NaOH solution at 15°C; (inset) SAED pattern corresponding to a ligament in part a; part b shows the smooth ligament surface morphology at a higher magnification. (c) HRTEM image shows lattice fringes extending throughout this ligament.

Figure 6. Tafel polarization curves of single-phase  $\alpha$ -Al solid solution and  $\text{Al}_2\text{Cu}$  intermetallics (a) in the 10 wt.% NaOH solution, (b) in the 5 wt.% HCl solution.

Figure 7.  $\text{N}_2$  isotherms at 77 K for the NPCRs by dealloying of melt-spun Al 32 at.% Cu alloy (a) in the 10 wt.% NaOH solution and (b) in the 5 wt.% HCl solution.



**Figure 1.** XRD patterns of melt-spun Al 32 at.% Cu alloy ribbons (a) before and (b-c) upon dealloying in the 5 wt.% HCl at 75°C and 10 wt.% NaOH solution at 15°C, respectively.



**Figure 2.** SEM images showing the microstructure of (a, b) quenching surface, and (c, d) free surface of NPCRs by dealloying of the Al 32 at.% Cu alloy in the 5 wt.% HCl solution at 75°C. Insets in parts b and d are their high-magnification images. (e) A typical EDX spectrum shows the composition of the resultant NPCRs.

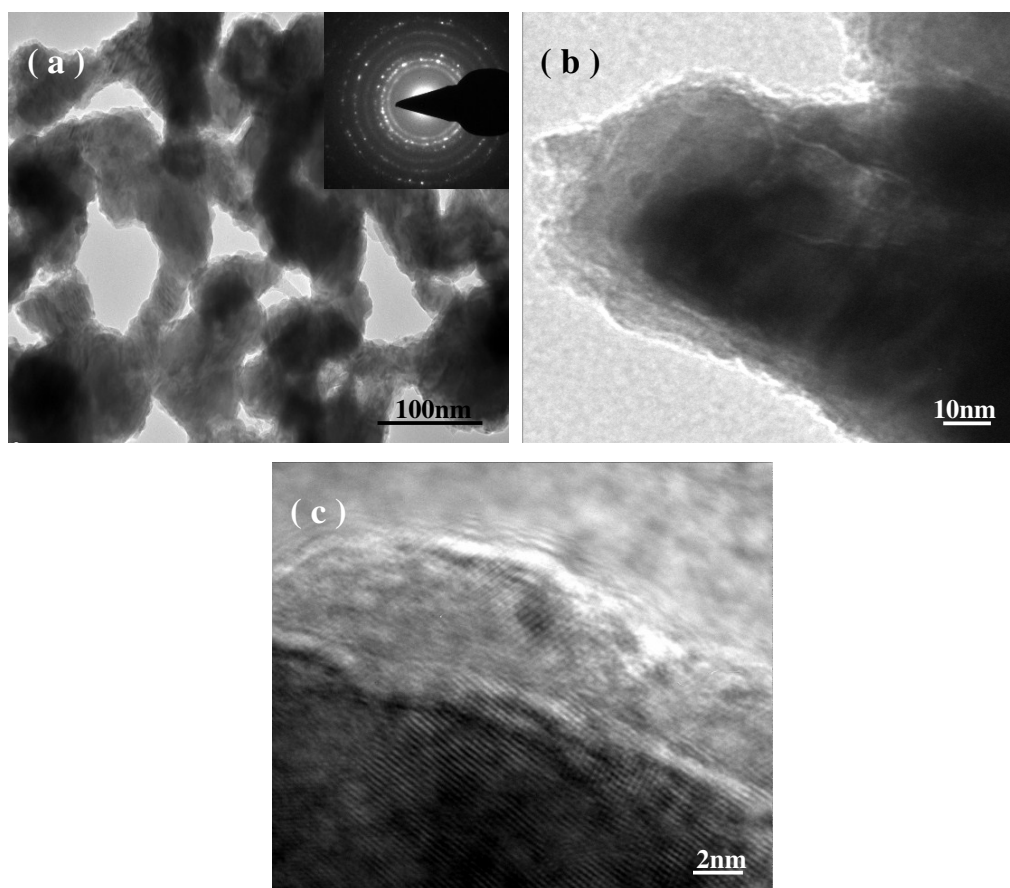


**Figure 3.** (a,b) TEM images show the porous structure in the channel walls of NPCRs by dealloying of melt-spun Al 32 at.% Cu alloy in the 5 wt.% HCl solution at 75°C; (inset) SAED pattern corresponding to a ligament in part a; part b shows the coarse ligament surface morphology at a higher magnification. (c) HRTEM image shows the crossed lattice fringes in the ligament.

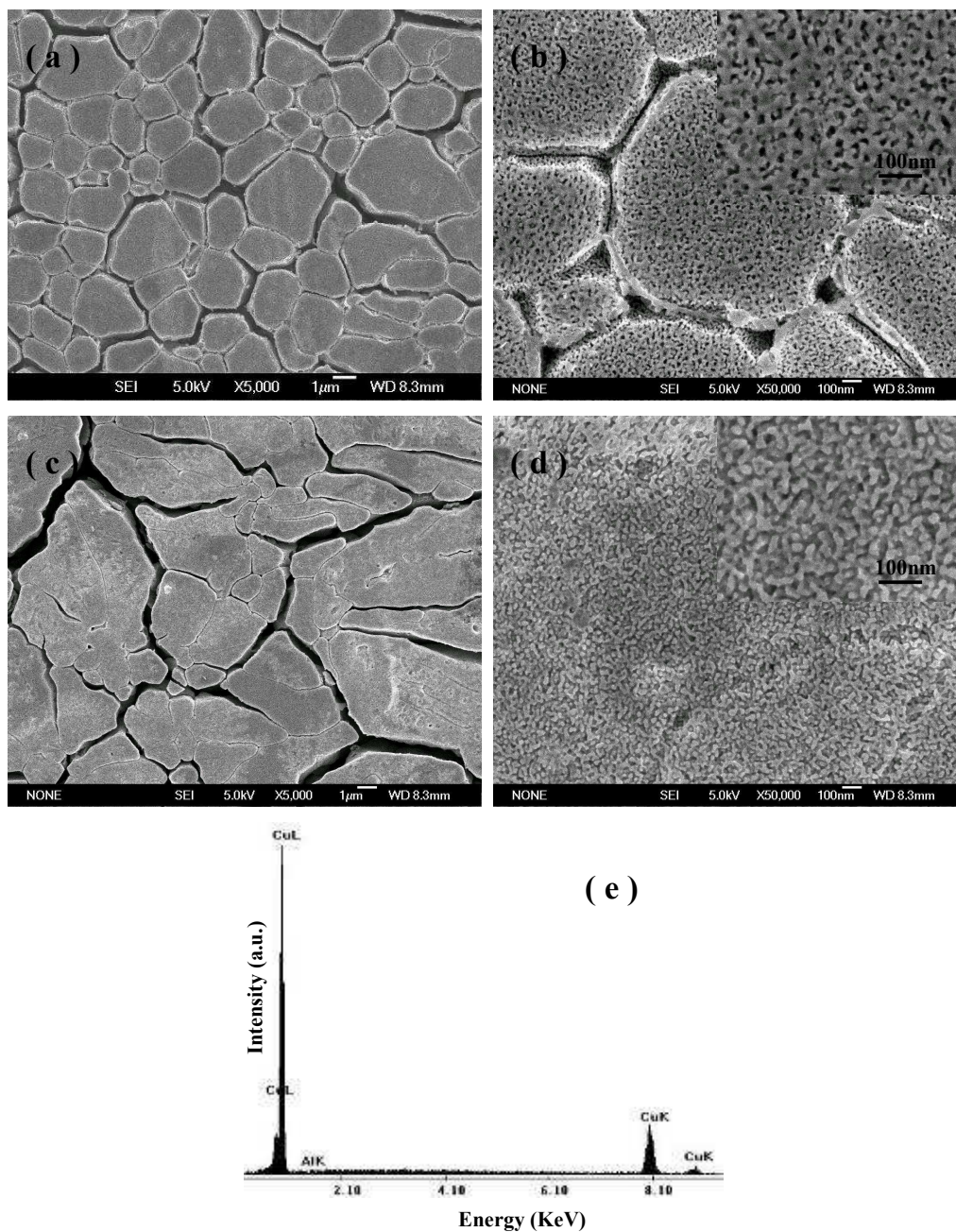


**Figure 4.** SEM images showing the microstructure of (a, b) quenching surface, and (c, d) free surface of NPCRs by dealloying of the Al 32 at.% Cu alloy in the 10 wt.% NaOH solution at 15°C. Insets in parts b and d are their high-magnification images. (e) A typical EDX spectrum shows the composition of the resultant NPCRs.

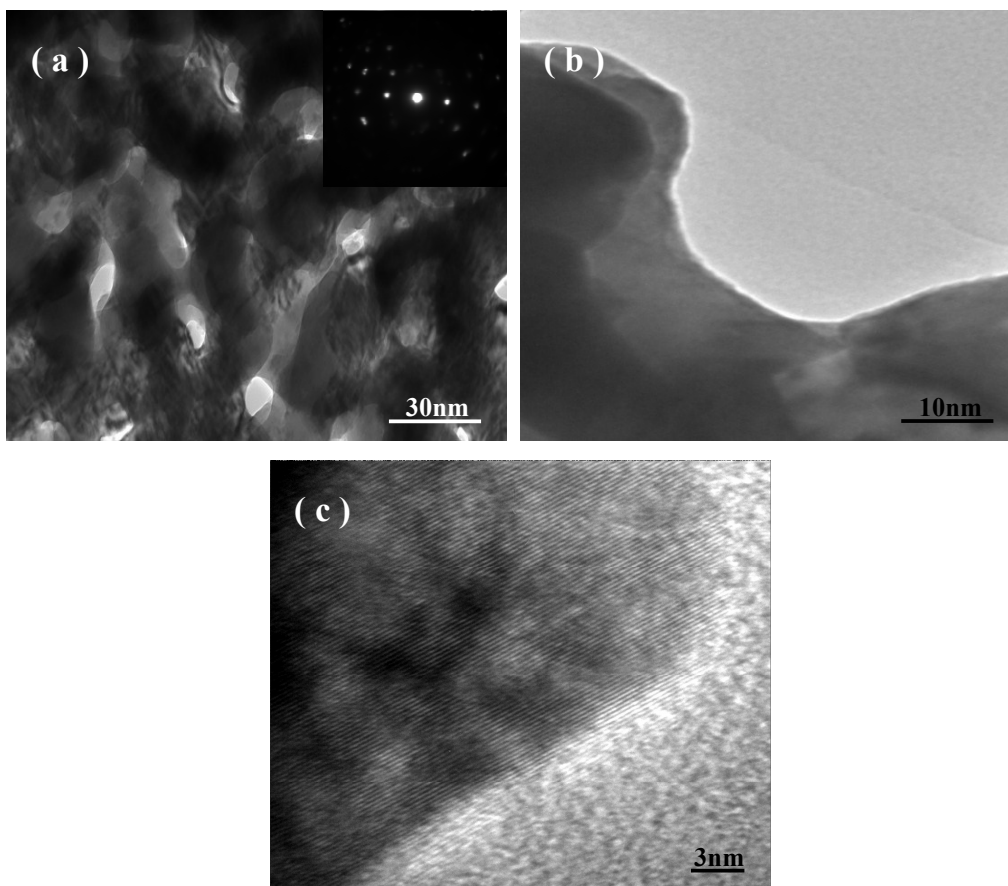


**Figure 5.** (a,b) TEM images show the porous structure in the channel walls of NPCRs by dealloying of melt-spun Al 32 at.% Cu alloy in the 10 wt.% NaOH solution at 15°C; (inset) SAED pattern corresponding to a ligament in part a; part b shows the smooth ligament surface morphology at a higher magnification. (c) HRTEM image shows lattice fringes extending throughout this ligament.

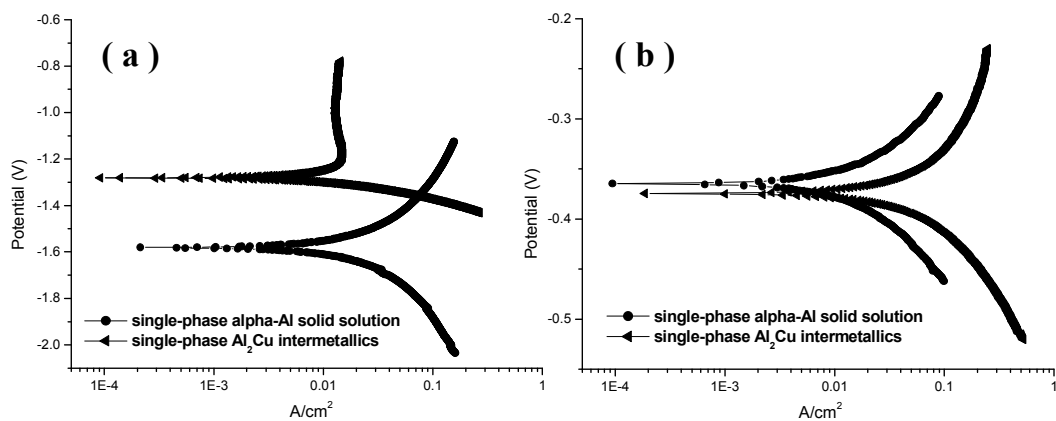


**Figure 6.** Tafel polarization curves of single-phase  $\alpha$ -Al solid solution and  $\text{Al}_2\text{Cu}$  intermetallics (a) in the 10 wt.% NaOH solution, (b) in the 5 wt.% HCl solution.

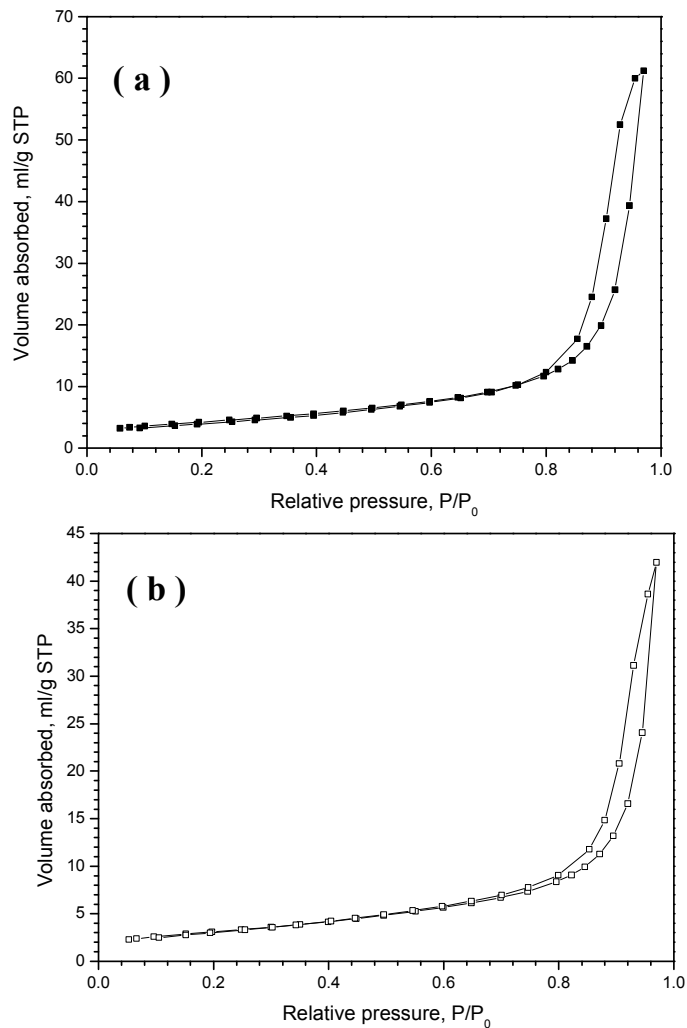


**Figure 7.** N<sub>2</sub> isotherms at 77 K for the NPCRs by dealloying of melt-spun Al 32 at.% Cu alloy (a) in the 10 wt.% NaOH solution and (b) in the 5 wt.% HCl solution.

